Journal of Physics: Conference Series **381** (2012) 012085 doi:10.1088/1742-6596/381/1/012085

Scattering of the halo nucleus ^{11}Li and its core ^{9}Li on ^{208}Pb at energies around the Coulomb barrier

M. J. G. Borge[1], M. Cubero[1,2], J. P. Fernández-García[3,4], L. Acosta[5], M. Alcorta[1], M. A. G. Alvarez[3,4], L. Buchmann[6], C. A. Diget[7], H. Al Falou[8], B. Fulton[7], H. O. U. Fynbo[9], D. Galaviz[1,10], J. Gómez-Camacho[4,3], R. Kanungo[8], J. A. Lay[3], M. Madurga[1], I. Mukha[3], T. Nilsson[11], A. M. Sánchez-Benítez[5], A. Shotter[6], O. Tengblad[1] and P. Walden[6]

1 Instituto de Estructura de la Materia, CSIC, 28006 Madrid, Spain
2 CICANUM, Universidad de Costa Rica, Apdo. 2060 San José, Costa Rica
3 Departamento FAMN, Universidad de Sevilla, 41080 Seville, Spain
4 Centro Nacional de Aceleradores, Universidad de Sevilla, 41092 Seville, Spain
5 Departamento de Física Aplicada, Universidad de Huelva, 21071 Huelva, Spain
6 TRIUMF, V6T2A3 Vancouver B.C., Canada
7 Department of Physics, University of York, YO 10 5DD Heslington, York, UK
8 Department of Astronomy and Physics, Saint Mary's University, Halifax, B3H3C3 Canada
9 Department of Physics and Astronomy, University of Aarhus, DK-8000, Århus, Denmark
10 CFNUL, Universidade de Lisboa, 1649-003 Lisbon, Portugal
11 Fundamental Physics, Chalmers University of Technology, 41296 Göteborg, Sweden

E-mail: mj.borge@csic.es

Abstract. The first measurement of the elastic scattering of the halo nucleus ^{11}Li and its core ^{9}Li on ^{208}Pb at energies around the Coulomb barrier is presented. The ^{11}Li reaction showed a large cross section for the breakup channel, even at energies well below the barrier. The analysis of the ^{11}Li + ^{208}Pb scattering data in terms of the continuum-discretized coupled-channel calculations indicates that the effect of the coupling to the breakup channels produces a strong suppression of the elastic cross section at energies above and below the barrier. This effect is mainly due to the strong Coulomb coupling to the dipole states in the low-lying continuum of ^{11}Li.

1. Introduction

Rutherford [1] inferred the structure of the atom from the reaction data measured by Geiger and Marsden [2], one century ago. Since then, nuclear structure properties have often been deduced from nuclear reaction studies. With the advent of the first accelerated radioactive beams new features in the nuclear structure were discovered. Twenty five years ago, Hansen and Jonson [3], interpreted the large interaction cross section observed in ^{11}Li by Tanihata [4] as a sign of a halo structure.

The halo structure is a threshold phenomenon due to the low binding energy of the last nucleons. The structure of halo nuclei has several features in common: a rather inert core, extended neutron distribution and very few bound excited states if any.

The discovery of the halo nuclei has brought renewed interest in the modeling of nuclear reactions. This structure will affect the reaction properties at near Coulomb barrier energies,

as for the very loosely bound system the model space should include the coupling between the bound states and the continuum.

Current approaches to reaction theory involve different approximations whose validity needs to be checked when applied to exotic nuclei. Our purpose was to study the reaction mechanisms of halo nuclei on the strong Coulomb field of the target at collision energies around the Coulomb barrier.

In this contribution we present the current status of the study of the scattering of the halo nucleus ^{11}Li and its core ^{9}Li on ^{208}Pb at energies around the Coulomb barrier. The most neutron-rich lithium isotope, ^{11}Li, is an intriguing case. It is the archetype of a Borromean halo nucleus, i.e. the two different binary subsystems, ^{9}Li-n and n-n, are unbound. Structurally it is composed of a ^{9}Li core and two weakly bound neutrons with S_{2n}=369.15(65) keV [5]. The density distribution of ^{11}Li extends well beyond its core, i.e., the rms matter radius for ^{9}Li is 2.44(6) fm, while for ^{11}Li it is 3.71(20) fm [6].

Due to the loosely bound structure, the neutron halo should be easily polarizable in the strong electric field of a heavy target such as ^{208}Pb. In fact, large soft electric dipole (E1) strength has been observed at low excitation energy in halo nuclei. This is in contrast to normal nuclei, where the E1 response is dominated by the giant dipole resonance at energies in the range of 10-20 MeV. The ^{11}Li has the strongest E1 transition ever observed at low excitation energy as determined in an exclusive measurement of the Coulomb dissociation of ^{11}Li at 70 MeV/u at RIKEN [7]. The B(E1) values are very sensitive to the structure model used to describe the halo nucleus. In experiments at these high energies it is difficult to get a good sensitivity at energies close to the break-up threshold.

Therefore it is interesting to obtain information of B(E1) by studying the dynamic of the halo nucleus ^{11}Li at Coulomb barrier energies on the intense electric field created by a ^{208}Pb target. This process can reveal new features of halo nuclei as predicted by [8]. For halo nuclei it is expected that collisions with heavy targets, in our case ^{208}Pb, at energies below the Coulomb barrier will depart from Rutherford scattering. This deviation can shed light on the structure of the ^{11}Li nucleus and it can give a hint on how the scattering process depends on the coupling to the continuum.

In order to disentangle the contribution of the loosely bound structure of ^{11}Li to the reaction process, one should know the behavior of the core, ^{9}Li, in the same conditions. No data exists for the scattering of ^{11}Li near the Coulomb barrier and for the scattering of ^{9}Li the data are scarce. The cross section of ^{9}Li on a 0.3 mg·cm^{-2} thick ^{208}Pb target was measured at 86 MeV [9], but this energy is three times the Coulomb barrier. Near the Coulomb barrier, the fusion cross section of ^{9}Li + ^{208}Pb was measured at center of mass (CM) energies from 23.9 to 43.0 MeV, and the "reduced" fusion excitation function was found to be similar for the A=7-9 Li isotopes [10]. Due to the lack of information on the ^{11,9}Li scattering on lead at energies around the Coulomb barrier we decided to study this process in detail to characterize the parameters of the potential describing the dynamic behavior of the ^{11}Li core, ^{9}Li, and use this information to extract the dipole polarizability contribution to the scattering of ^{11}Li.

2. Experimental Setup

The experiment was performed in the post-accelerated ISAC-II line at the TRIUMF facility (Vancouver, Canada). A primary 100 μA proton beam of 500 MeV [11] produced at the TRIUMF cyclotron impinged on a Ta primary target. The Li secondary beams were transported to the ISAC-II facility for post acceleration. The intensity of the ^{9}Li beam on the Pb-target was higher than 10^5 pps and prevented us from using a monitor detector. The average intensity of the ^{11}Li beam as detected in our monitor detector ($\Omega = 3\times10^{-4}$ of 4π) placed 280 mm downstream was 4×10^3 ^{11}Li/s.

The setup was designed keeping in mind the expected low intensity of the ^{11}Li beam, and the

fact that we were interested in separating the elastically scattered ^{11}Li ions from the fragments, being the most probable one, ^{9}Li. So we decided to use telescopes with the thinest front detectors to achieve mass separation of the fragments. These detectors did not have cylindrical symmetry, so the analysis had to be done pixel by pixel. To increase the statistics the backward angle detectors were placed closer to the target. The angular coverage of the telescopes was chosen to take into account the region where the differential cross section for the elastic scattering of the halo nucleus ^{11}Li with lead vary, at most, depending of the ingredients included in the model predictions.

The setup used consisted of four telescopes as illustrated in figure 1. The rings on the DSSSD1 and DSSSD2 indicates the axial symmetry of the scattering process. In the forward direction we had two telescopes, T1 and T2, each one consisting of a windowless 40 μm thick Double-Sided Silicon Strip Detector (DSSSD) [12] of 16×16 strips acting as ΔE detector, and a 500 μm thick PAD as E detector. Both DSSSDs were placed at a distance in its central part of 80 mm from the target covering different angles: telescope T1 from 10° to 40° and telescope T2 from 30° to 60°. Telescopes T3 and T4 consisted of a 20 μm thick ΔE Single-Sided Silicon Strip Detector (SSSD) of 16 strips and a 60 μm thick DSSSD behind. The SSSD's of T3 and T4 were placed at 52 mm from the target with 7.5 mm to the back DSSSD detectors. Telescope T3 covered from 50° to 100° and telescope T4 from 90° to 140°. The ^{208}Pb target was tilted 75° with respect to the beam direction. Two different target thickness were used, 1.45 and 1.9 mg·cm^{-2} of ^{208}Pb for the ^{9}Li study. As far as the intensity of the ^{11}Li beam was reasonable only the thin 1.45 mg·cm^{-2} ^{208}Pb target was used in order to minimize the losses in resolution due to the straggling in the target.

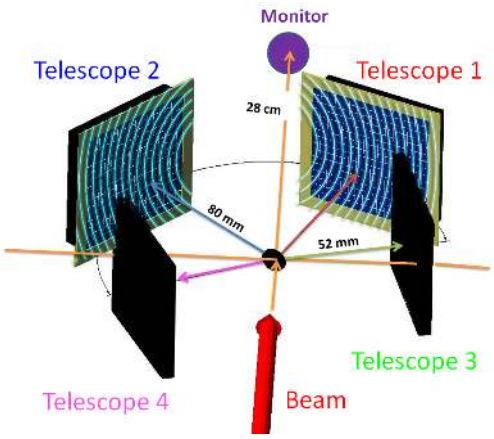

Figure 1. *(color online) Schematic view of the experimental setup. The angular coverage of each telescope from T1 to T4 is: 10°-40°, 30°-60°, 50°-100° and 90°-140°, respectively.*

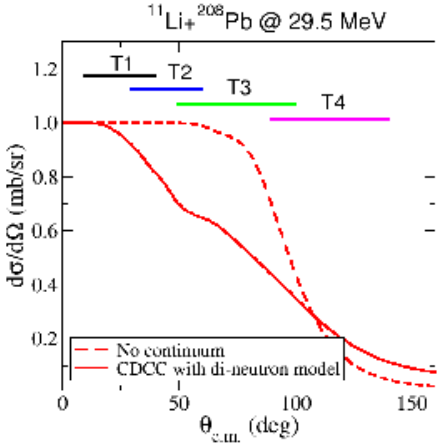

Figure 2. *Expected CDCC differential elastic cross section relative to Rutherford of ^{11}Li on ^{208}Pb at 29.5 MeV. The coverage of each telescope is indicated in the upper part.*

The segmentation of the detector system allows to get information of 256 pixels (16×16) per telescope either by matching front and back strips of the DSSSD for telescopes 1 and 2, or front and back detectors in telescopes 3 and 4. In total 1024 micro-detectors were analyzed. Due to the different distances between telescopes and target the angular coverage per pixel is 2-3° for T1 and T2 and for the telescopes T3 and T4 between 3-4°. This configuration gave rise to large angular coverage with high resolution.

Figure 2 shows two calculations for the expected differential elastic cross section relative to Rutherford of ^{11}Li on ^{208}Pb at the near barrier energy of E_{lab} = 29.5 MeV ($V_b \approx$ 28 MeV),

obtained with the Continuum-Discretized Coupled-Channels (CDCC) method. The dashed line is the calculation in which one takes into account the spatial extension of the ^{11}Li nucleus within a simple two-body di-neutron model. The solid line is the full CDCC calculation, based on the same di-neutron model, including the nuclear and Coulomb couplings to the breakup channels. The angular coverage of each telescope is indicated in the upper part of the figure 2.

3. Analysis and Results

The differential elastic cross section of a ^{11}Li beam on a 1.45 mg·cm^{-2} thick ^{208}Pb target was measured in this work for the first time at the laboratory energies around the Coulomb barrier of 24.2 and 29.7 MeV. To characterize the behaviour of the core, the ^{9}Li + ^{208}Pb scattering was also measured with the same setup and at the same CM energies, 23.0 and 28.2 MeV. No previous data on the elastic scattering of the ^{9}Li + ^{208}Pb system exist in the literature at energies close to the Coulomb barrier. The experimental results are analyzed in the framework of the optical model (OM) and also using a CDCC analysis.

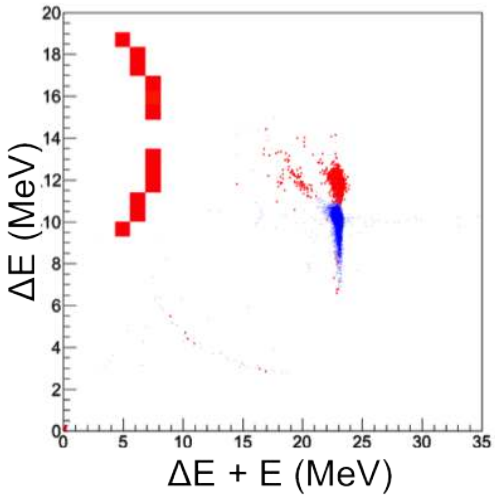

Figure 3. *(color online) Two-dimensional plot of ΔE versus ΔE + E. The ^{9}Li (in blue) and the ^{11}Li + ^{208}Pb (in red) scattering data at 23.0 MeV CM energy.*

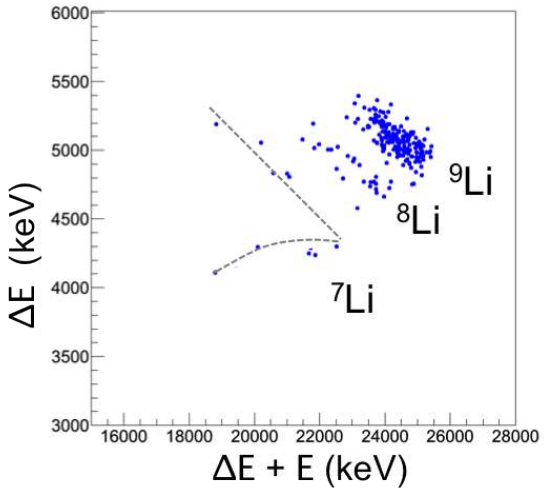

Figure 4. *Two-dimensional plot of ΔE versus ΔE + E for ^{9}Li + ^{208}Pb scattering data at the CM energy of 28.2 MeV for a pixel at 128.2°. Notice the presence of breakup channels already at this energy.*

The data of the ^{11}Li scattering on lead were accumulated during 82.2 h for the 24.2 MeV ^{11}Li beam energy and 118.12 h for the 29.7 MeV energy. No electronic shifting occurred during the data taking. For energy calibration both external alpha sources (^{148}Gd, ^{239}Pu, ^{241}Am and ^{244}Cm) and the elastic peak of ^{9}Li and ^{11}Li for CM energy of 23.0 MeV were used. The events were selected in the following way. Individual thresholds were chosen for each strip. A time condition selected by the TDC was applied. When two neighbour strips were fired the event was disregarded to avoid charge sharing [13]. To select heavy ion signals and avoid beta contributions, a condition in the energy deposited in the front and back strips forming the pixel was applied for the DSSSD, $\Delta E_{diff} \leq 70$ keV. For more details, see [14].

The data were first analyzed assuming that the detectors T1 and T2 were at the position determined by the geometrical measurements, and the optical beam axis centered in the ^{208}Pb target. Due to the close geometry of the setup, a refined determination of the angle subtended by each pixel was done based on the fact that the elastic scattering of ^{9}Li on ^{208}Pb at energies below the barrier should follow the Rutherford behaviour at forward angles. The differential elastic cross section with optimized position vectors for each detector was calculated by the

average of the counts in each pixel and divided by the solid angle of the pixel corresponding to a certain angular ring. The angles covered by the T3 and T4 telescopes were determined only by geometrical considerations as the angular dependence of the cross section is less steep.

Elastic events were selected in the two-dimensional plot of ΔE versus ΔE + E energy spectra for each pixel. A clear identification of the elastic peaks and fragments, both in the ^{9}Li and in the ^{11}Li scattering data, was achieved. Figure 3 illustrates the data obtained for ^{9}Li and ^{11}Li beams scattered on the same 1.45 mg·cm^{-2} thick ^{208}Pb target and at equivalent CM energies of 23.0 MeV. The two-dimensional plot shows overlay the ^{9}Li scattering data in blue with the ^{11}Li scattering data, in red. For the latter the contribution of the elastic and the ^{9}Li breakup channel are clearly observed and separated. The pixels included in the selected angular ring of (19.5±1.0)° are shown on the left corner of figure 3. It is surprising the relatively large contribution of the breakup channel observed at this low energy and forward angle. The ^{9}Li scattering data are given only for one of the pixels centered at 18.5°. One can notice the presence of some α-particles probably due to the ^{9}Li β-decay that has a 50 % probability of decaying into 2α. We show In figure 4 the two-dimensional plot corresponding to ^{9}Li + ^{208}Pb scattering data at a CM energy of 28.2 MeV and for a pixel of telescope 4 centered at 128.2°. It is remarkable that at this very near threshold energy one can identify the breakup of the ^{9}Li + ^{208}Pb system into ^{8}Li + ^{209}Pb ($Q = -0.1$ MeV) and the possible contribution of ^{7}Li + ^{210}Pb ($Q = 3$ MeV). The contribution of these channels has been analyzed and removed in order to extract the elastic cross section. These contributions were not identified in the preliminary analysis of the data given in [14].

4. Discussion and Conclusions

Figure 5 shows on the left the differential elastic cross section relative to Rutherford for ^{9}Li on ^{208}Pb at energies below the barrier. We notice that the behaviour of the cross section with the angle follows the usual Fresnel pattern which characterizes the elastic scattering between heavy ions at Coulomb barrier energies, and can be described with an optical model potential with standard parameters [14].

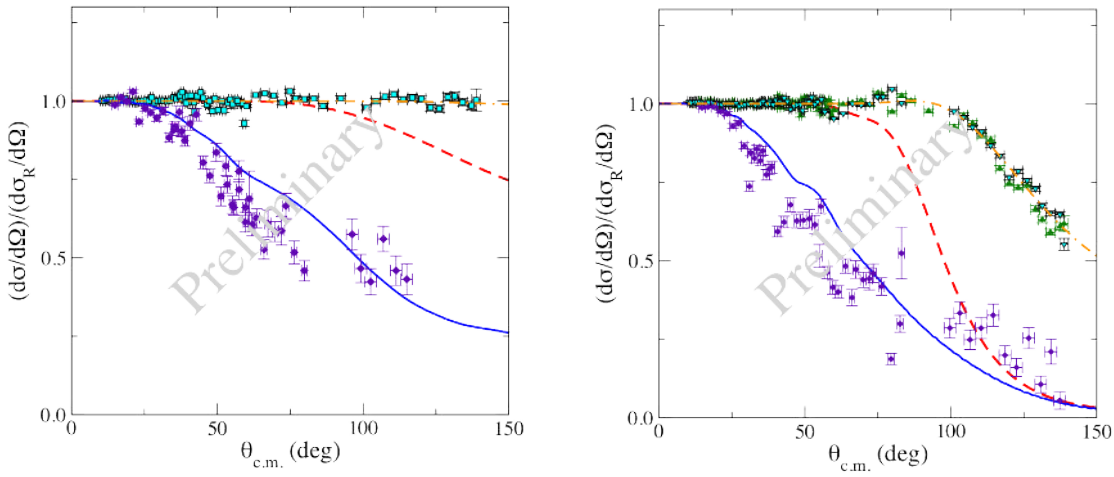

Figure 5. *(color online) Differential elastic cross section of ^{9}Li and ^{11}Li on ^{208}Pb for CM energies of 23.0 MeV on the left, and 28.2 MeV on the right. The results obtained for ^{9}Li on ^{208}Pb are given for both targets. For details on the calculations see text.*

On the other hand, the ^{11}Li elastic scattering on ^{208}Pb at the same CM energy of 23.0 MeV shows a smooth angular dependence and a strong suppression with respect to the Rutherford cross section (see figure 5). To understand this behaviour these data have been compared with

CDCC calculations, which take into account the large spatial extension of the ^{11}Li nucleus and the coupling to the breaukup channels. Due to its Borromean structure, the ^{11}Li nucleus should be described, at least, within a three-model, ^{9}Li + n + n, therefore, the treatment of the ^{11}Li + ^{208}Pb reaction involves a four-body scattering problem. This kind of calculations have been performed for ^{6}He + ^{208}Pb using an extension of the CDCC method [15]. However, the elastic scattering could be also very well described using a two-body model for ^{6}He (α+2n), provided that the 2n-core wavefunction reproduces the correct size of the ^{6}He system [16]. Given the complexity of the four-body CDCC calculations, we adopt here also a two-body model for the ^{11}Li nucleus (^{9}Li+2n), and hence treat the scattering process within a three-body framework. The 2n-^{9}Li interaction is parametrized using a Woods-Saxon potential. The parameters of this potential, as well as the effective separation energy of the two clusters, are adjusted to reproduce the 3-body ground state density probability at the relevant distances ($r < 4$ fm). The resulting parameters of the Woods-Saxon potential are V_0 = -39.03 MeV, $R_0 = 2.7$ fm, and $a = 0.30$ fm. The effective separation energy is $S_{2n-^{9}Li} = 0.54$ MeV, which differs from the experimental two-neutron separation $S_{2n} = 0.369$ MeV [5], since we freeze certain degrees of freedom. This model yields a root-mean-squared (rms) separation between the two clusters of $\langle r_{2n-^{9}Li}\rangle = 5.09$ fm, which is very close to the value obtained in the ^{11}Li three-body model. By contrast, when one takes for the 2n-^{9}Li system the ^{11}Li two-neutron separation energy, one gets a distance of 5.79 fm. Furthermore, this interaction is able to reproduce the B(E1) distribution obtained at RIKEN by Nakamura *et al.* [7].

In addition to the structure model, the other physical ingredients that enter the CDCC calculation are the cluster-target optical potentials, ^{9}Li + ^{208}Pb and 2n + ^{208}Pb. The real part of the ^{9}Li + ^{208}Pb potential was generated microscopically using the double-folding São Paulo potential (SPP) [17], with the ^{9}Li matter density from Ref. [6] and the ^{208}Pb density from a Hartree-Fock calculation. The corresponding rms values are 2.44(6) fm and 5.53 fm, respectively. The imaginary part was parametrized using a Woods-Saxon potential. The parameters of the Woods-Saxon potential W_i, r_i and a_i as well as the normalization of the real part N_r were taken as adjustable parameters in order to reproduce the present ^{9}Li elastic data at $E_{\rm lab}$=29.7 MeV. These optical model calculations were performed with the coupled-channels code FRESCO [18], and further details can be found in [14]. The 2n-^{208}Pb potential was generated by means of a single-folding procedure, by folding the neutron-target interaction, taken from the compilation of Perey and Perey [19], with the n-n density obtained from the three-body calculation of the ^{11}Li nucleus.

The elastic ^{11}Li + ^{208}Pb data for energies below and around the Coulomb barrier are compared in figure 5 with CDCC calculations with (continuous line) and without (dashed line) coupling to the continuum.

The experimental data for the elastic scattering of ^{11}Li + ^{208}Pb, shown in figure 5, display a strong reduction with respect to Rutherford, over the whole angular range, at both energies. This is remarkably different to the behaviour of the data for ^{9}Li, which behaves as a "normal" nucleus, following the Rutherford formula at all angles at energies below the barrier ($E_{\rm lab}$ = 24.2 MeV), while at energies above the barrier deviates from Rutherford at angles beyond the grazing angle.

The special behavior of ^{11}Li is associated to the effect of Coulomb Dipole Polarizability [8]. The weakly bound ^{11}Li, in the strong Coulomb field of the target, gets distorted and eventually breaks up. This reduces the elastic cross sections in a similar pattern below ($E_{\rm CM} = 23.0$ MeV) and around ($E_{\rm CM} = 28.2$ MeV) the Coulomb barrier, where it is remarkable the absence of a well defined grazing angle. CDCC calculations, that take into account both the effects of Coulomb and nuclear break-up, reproduce satisfactorily this reduction.

In summary: we present here the first measurement of the elastic scattering of the halo nucleus ^{11}Li and its core ^{9}Li on ^{208}Pb at energies below and around the Coulomb barrier. The

^{9}Li + ^{208}Pb scattering data behave with the angle as expected and the differential cross section can be well described within the framework of the optical model. The strong reduction of the ^{11}Li + ^{208}Pb elastic cross section observed both below and around the Coulomb barrier, along with the corresponding increase in the break-up cross section, depends strongly on the Coulomb dipole coupling of the ground state to low energy continuum states in ^{11}Li. A consistent analysis of the elastic and the break-up differential cross sections, currently in progress, will allow us to obtain accurate information of the values of the B(E1) distribution at energies close to the break-up threshold.

References

[1] Rutherford E 1911 *Philos. Mag* **6** 21
[2] Geiger H and Marsden E 1909 *Roy. Soc. Proc. A* **82** 495–500
[3] Hansen P G and Jonson B 1987 *Euro. Phys. Lett.* **4** 409
[4] Tanihata I, Hamagaki H, Hashimoto O, Shida Y, Yoshikawa N, Sugimoto K, Yamakawa O, Kobayashi T and Takahashi N 1985 *Phys. Rev. Lett.* **55** 2676
[5] Smith M, Brodeur M, Brunner T, Ettenauer S, Lapierre A, Ringle R, Ryjkov V L, Ames F, Bricault P, Drake G W F, Delheij P, Lunney D, Sarazin F and Dilling J 2008 *Phys. Rev. Lett.* **101** 202501
[6] Dobrovolsky A V, Alkhazov G D, Andronenko M N, Bauchet A, Egelhof P, Fritz S, Geissel H, Gross C, Khanzadeev A, Korolev G, Kraus G, Lobodenko A A, Munzenberg G, Mutterer M, Neumaier S R, Schfer T, Scheidenberger C, Seliverstov D M, Timofeev N A, Vorobyov A A and Yatsoura V I 2006 *Nuc. Phys.* **A766** 1
[7] Nakamura T, Vinodkumar A M, Sugimoto T, Sugimoto T, Aoi N, Baba H, Bazin D, Fukuda N, Gomi T, Hasegawa H, Imai N, Ishihara M, Kobayashi T, Kondo Y, Kubo T, Miura M, Motobayashi T, Otsu H, Saito A, , Sakurai H, Shimoura S, Watanabe K, Watanabe Y X, Yakushiji T, Yanagisawa Y and Yoneda K 2006 *Phys. Rev. Lett.* **96** 252502
[8] Andrés M V and Gómez-Camacho J 1999 *Phys. Rev. Lett.* **82** 1387
[9] Skobelev *et al* N K 1992 *Z. Phys. A* **341** 315
[10] Vinodkumar A M, Loveland W, Sprunger P H, Prisbrey L, Trinczek M, Dombsky M, Machule P, Kolata J J and Roberts A 2009 *Phys. Rev. C* **80** 054609
[11] Ball G, Buchmann L, Davids B, Kanungo R, Ruiz C and Svensson C E 2011 *J. Phys. G* **38** 024003
[12] Tengblad O, Bergmann U C, Fraile L M, Fynbo H O U and Walsh S 2004 *Nucl. Inst. Meth. Phys. Res.* **A525** 458
[13] Bergmann U C, Fynbo H O U and Tengblad O 2003 *Nucl. Instrum. Meth.* **A515** 657
[14] Cubero M, Fernández-García J P, Acosta J A L L, Alcorta M, Álvarez M M M A G, Borge M J G, Diget L B C A, Fulton B, Fynbo H O U, Galaviz D, Gómez-Camacho J, Martel I, Moro A M, Mukha I, Nilsson T, Sánchez-Benítez A M, Shotter A, Tengblad O and Walden P 2011 *Eur. Phys. J, web of conf* **17** 16002
[15] Rodríguez-Gallardo M, Arias J M, Gómez-Camacho J, Johnson R C, Moro A M, Thompson I J and Tostevin J A 1996 *Phys. Rev. C* **54** 117
[16] Acosta L, Sánchez-Benítez A M, Gómez M E, Martel I, Pérez-Bernal F, Pizarro F, Rodríguez-Quintero J, Rusek K, Álvarez M A G, Andrés M V, Espino J M, Fernández-García J P, Gómez-Camacho J, Moro A, Angulo C, Cabrera J, Casarejos E, Demaret P, Borge M J G, Escrig D, Tengblad O, Cherubini S, Figuera P, Gulino M, Freer M, Metelko C, Ziman V, Raabe R, Mukha I, Smirnov D, Kakuee O and Rahighi J 2011 *Phys. Rev. C.* **84** 044604
[17] Chamon L C, Carlson B V, Gasques L R, Pereira D, Conti C D, Alvarez M A G, Hussein M S, Ribeiro M A C, E S Rossi J and Silva C P 1997 *Phys. Rev. C* **66** 14610
[18] Thompson I 1988 *Computer Phys. Rep.* **7** 167
[19] Perey C M and Perey F G 1963 *Phys. Rev.* **132** 755